Regulation of glutamate receptor internalization by the spine cytoskeleton is mediated by its PKA-dependent association with CPG2

Sven Loebrich[a], Biljana Djukic[b], Zachary J. Tong[a], Jeffrey R. Cottrell[a,c], Gina G. Turrigiano[b,1], and Elly Nedivi[a,c,d,1]

[a]Picower Institute for Learning and Memory and Departments of [d]Biology and [c]Brain and Cognitive Sciences, Massachusetts Institute of Technology, Cambridge, MA 02139; and [b]Department of Biology, Brandeis University, Waltham, MA 02453

Contributed by Gina G. Turrigiano, October 9, 2013 (sent for review June 27, 2013)

A key neuronal mechanism for adjusting excitatory synaptic strength is clathrin-mediated endocytosis of postsynaptic glutamate receptors (GluRs). The actin cytoskeleton is critical for clathrin-mediated endocytosis, yet we lack a mechanistic understanding of its interaction with the endocytic process and how it may be regulated. Here we show that F-actin in dendritic spines physically binds the *synaptic nuclear envelope 1* gene product candidate plasticity gene 2 (CPG2) in a PKA-dependent manner, and that this association is required for synaptic GluR internalization. Mutating two PKA sites on CPG2 disrupts its cytoskeletal association, attenuating GluR endocytosis and affecting the efficacy of synaptic transmission in vivo. These results identify CPG2 as an F-actin binding partner that functionally mediates interaction of the spine cytoskeleton with postsynaptic endocytosis. Further, the regulation of CPG2/F-actin association by PKA provides a gateway for cellular control of synaptic receptor internalization through second messenger signaling pathways. Recent identification of human *synaptic nuclear envelope 1* as a risk locus for bipolar disorder suggests that CPG2 could play a role in synaptic dysfunction underlying neuropsychiatric disease.

AMPA receptor | synapse

Clathrin-mediated endocytosis (CME) is one of several mechanisms for retrieving plasma membrane constituents and transmembrane proteins from the cell surface (reviewed in ref. 1). Models in yeast and mammals have implicated F-actin in various stages of CME, including vesicle formation, scission, and propulsion away from the surface membrane (reviewed in ref. 2). Actin polymerization has been observed at hot spots of CME where it peaks shortly after vesicle scission, and coordinated actin nucleation and recruitment of membrane binding proteins seems to be crucial for CME (3). However, despite these recurring indications, the mechanisms by which the F-actin cytoskeleton implements endocytosis, and the regulatory molecules involved, remain elusive.

At the synapse, CME of AMPA-type glutamate receptors (AMPARs) from the postsynaptic membrane is thought to be the substrate for various forms of plasticity, including long-term depression (LTD). AMPAR internalization by CME (4, 5) occurs constitutively and in an activity-dependent manner in response to agonist application and during some forms of LTD (6, 7). Indirectly, CME is also important for the expression of long-term potentiation (LTP), because recycling endosomes are the source of AMPARs inserted into the surface membrane during LTP (8). Although previous studies suggest that the actin cytoskeleton plays a role in internalization of AMPAR and the control of synaptic strength, the molecular mechanisms mediating this process and their regulation remain unknown.

AMPAR internalization is regulated by a number of genes, including candidate plasticity gene 2 (*Cpg2*), first identified in a screen for activity-regulated genes in the nervous system (9). *Cpg2,* a transcript of the *synaptic nuclear envelope 1* (*Syne1*) gene, encodes a 102-kDa protein that regulates constitutive and activity-induced internalization of synaptic glutamate receptors. Structurally, CPG2 shows homology to dystrophin (10) and spectrin (11), both F-actin–binding proteins. Given its role in glutamate receptor internalization and the elements in its primary structure suggesting association with F-actin, we tested the hypothesis that CPG2 constitutes a molecular link coupling CME to the cytoskeleton in dendritic spines. Our results identify CPG2 as essential for functional coupling of synaptic AMPAR CME with the spine cytoskeleton and a key integration point for PKA signaling in the synaptic endocytic process.

Results

CPG2 Binds F-Actin in Vitro Through a Novel Bipartite Association Domain. CPG2 localizes specifically to dendritic spines (11) adjacent to but discrete from the postsynaptic density (PSD) and embedded within the F-actin cytoskeleton (Fig. 1*A*). Protein domain prediction algorithms identify a putative spectrin repeat near the CPG2 N terminus (Fig. 1*B*). Spectrin repeats are a hallmark of the spectrin protein superfamily, many of which physically associate with the F-actin cytoskeleton (reviewed in ref. 12). The CPG2 protein sequence also features three predicted coiled-coil regions, potentially representing protein–protein interaction motifs. CPG2 proximity to the F-actin cytoskeleton and its predicted spectrin repeat led us to investigate whether it associates with F-actin and whether this association may be linked to CPG2's role in glutamate receptor endocytosis.

To test for CPG2 binding to F-actin we first performed an in vitro actin binding assay (13). CPG2, in vitro transcribed and

Significance

Clathrin-mediated endocytosis (CME) of glutamate receptors from the postsynaptic membrane is central for adjusting synaptic strength and is thought to be the substrate for various forms of synaptic plasticity. The role of the actin cytoskeleton in CME is recognized as fundamental but remains poorly understood, and we lack a mechanistic understanding of the cytoskeletal/CME association, its functional consequences, and its regulation. Here we identify the activity-regulated *synaptic nuclear envelope 1* gene product candidate plasticity gene 2 (CPG2) as a direct functional link between the cytoskeleton and postsynaptic endocytosis, and as a nexus for the interaction of signaling pathways with the endocytic process. CPG2 reversibly associates with F-actin, and this association is positively regulated by PKA and is an important regulator of both glutamate receptor internalization and postsynaptic strength.

Author contributions: S.L., B.D., G.G.T., and E.N. designed research; S.L., B.D., Z.J.T., and J.R.C. performed research; S.L. and B.D. analyzed data; and S.L., G.G.T., and E.N. wrote the paper.

The authors declare no conflict of interest.

[1]To whom correspondence may be addressed. E-mail: turrigiano@brandeis.edu or nedivi@mit.edu.

This article contains supporting information online at www.pnas.org/lookup/suppl/doi:10.1073/pnas.1318860110/-/DCSupplemental.

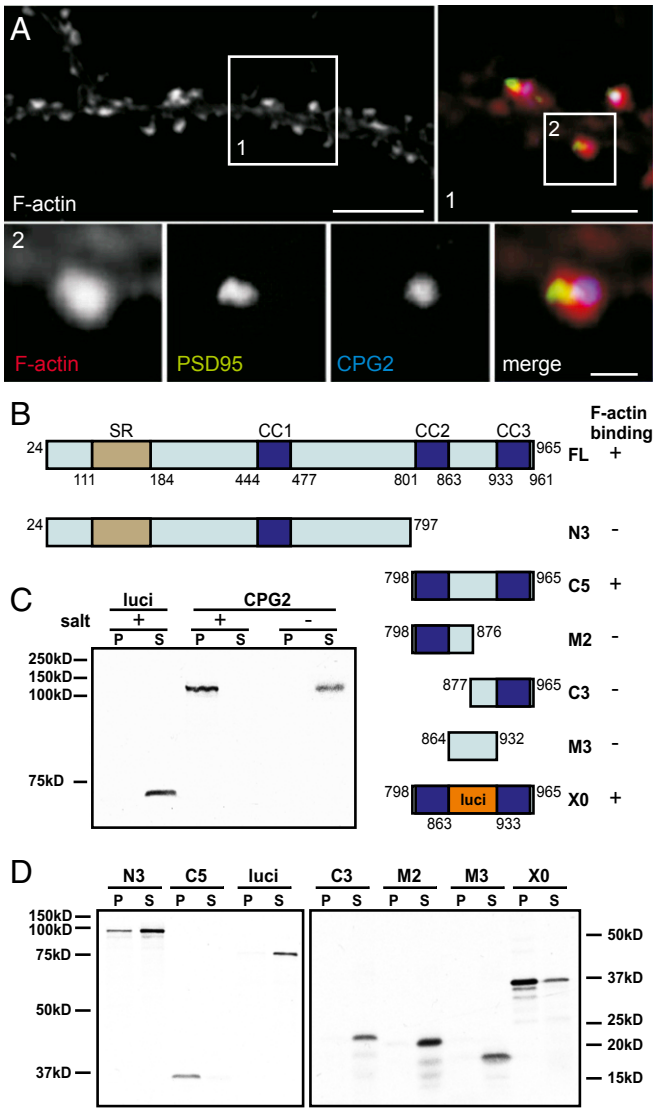

Fig. 1. CPG2 interacts with actin via a novel bipartite F-actin association domain. (*A*) Immunocytochemistry on cultured hippocampal neurons. (*Upper Left*) Black-and-white image of rhodamine phalloidine staining of F-actin in a dendritic segment. Box 1 is magnified and shown in color (*Upper Right*). F-actin is depicted in red, PSD95 in green, and CPG2 in blue. (*Lower*) Magnified view of box 2. (Scale bars: 10 μm, *Upper Left*; 4 μm, *Upper Right*; 2 μm, *Lower*.) (*B*) Schematic of CPG2 protein and its predicted motifs. A spectrin repeat and three coiled-coil domains (CC1–3) are annotated. Association with actin filaments is indicated by + and lack thereof by −. (*C*) Autoradiography of ^{35}S-labeled FL CPG2 or luciferase (luci). P, pellet fraction; S, supernatant. Presence or absence of salt is depicted by + or −, respectively. (*D*) Molecular dissection of the CPG2 C terminus. Autoradiography of the various truncated constructs depicted in *B* is shown.

translated in the presence of [^{35}S]methionine, was mixed with monomeric actin. Addition of ATP and salt causes F-actin polymerization and formation of filaments that can be sedimented by ultracentrifugation, together with any bound actin-associated proteins (Fig. 1*C*). Full-length (FL) CPG2 was found in the actin pellet only after addition of salt, suggesting that it physically associates with actin filaments. Non-F-actin–binding proteins such as luciferase were found exclusively in the supernatant.

We next tested protein deletion fragments of CPG2 for actin binding. A 773-aa N-terminal fragment (N3) containing the spectrin repeat as well as the first coiled-coil remained mostly soluble after mixing with F-actin. In contrast, the complementary C-terminal fragment (C5) containing the last two coiled-coils (CC2 and CC3) cosedimented with F-actin in the pellet (Fig. 1*D*). Further dissection of the C terminus showed that F-actin binding is lost in fragments containing only one, or neither, of the two C-terminal coiled-coils (Fig. 1 *B* and *D*, fragments M2, C3, and M3), suggesting that both coiled-coil domains are necessary for CPG2 association with F-actin. A chimeric fragment containing both C-terminal coiled-coil domains separated by exogenous luciferase protein sequence matching the M3 fragment in length (X0) readily bound F-actin. Hence, CPG2 does not bind to actin through its predicted spectrin domain. Instead, the two CPG2 C-terminal coiled-coils comprise a novel bipartite binding domain that is necessary and sufficient for CPG2 association with F-actin in vitro.

Binding to the F-Actin Cytoskeleton Anchors CPG2 in Dendritic Spines. We confirmed CPG2 association with the spine cytoskeleton using an in vivo actin-binding assay. Mild extraction of live cells with ice-cold 0.5% Triton solution leads to solubilization of the plasma and internal membranes. The bulky F-actin cytoskeleton and associated proteins withstand this extraction. Hippocampal neurons cultured for 21 d in vitro were fixed with (+) or without (−) prior extraction (Fig. 2 *A*–*C*). F-actin in spine heads was detected by rhodamine phalloidin staining whereas SV2, a transmembrane protein on synaptic vesicles, was almost completely lost (98.3 ± 0.2% before extraction vs. 1.2 ± 0.1% following extraction, Fig. 2 *A* and *C*). CPG2 immunoreactivity persisted following extraction and remained localized within spines (91.7 ± 4.7% before vs. 88.6 ± 3.5% after extraction, Fig. 2 *B* and *C*), with no significant difference in the percentage of spines containing CPG2 with or without extraction (Fig. 2*C*). CPG2, but not PSD95, was lost from dendritic spines upon depolymerization of F-actin by latrunculin (Fig. S1), further demonstrating that CPG2 associates with the spine cytoskeleton in vivo.

To test whether the F-actin association domain identified in vitro mediates CPG2's cytoskeletal attachment in neurons we used a knockdown and replacement strategy (14). Three independent small hairpin RNAs were found to significantly decrease CPG2 immunoreactivity and protein levels, by 85% or greater (Fig. S2). A cassette expressing one of these hairpins under control of the U6 promoter was inserted into a lentiviral vector, adjacent to a second cassette expressing EGFP fused to FL CPG2, the CPG2 N3, or CPG2 C5 fragment, driven by the Ubiquitin promoter. These GFP-fusion cDNAs were rendered knockdown-resistant by two silent mutations, allowing effective replacement of endogenous CPG2 (Fig. 2*D*). The GFP–FL CPG2 fusion protein, detected by antibodies against either GFP or CPG2, was enriched in spine heads and colocalized with F-actin (Fig. 2*E*, *Upper*). The percentage of spines positive for GFP–FL CPG2 was 94.2 ± 0.8%, comparable to those with endogenous CPG2 (Fig. 2*G*). The replacement GFP–FL CPG2 protein was resistant to Triton extraction, suggesting that like endogenous CPG2 it physically associates with the actin cytoskeleton (94.3 ± 1.1% after extraction, Fig. 2*E*, *Lower*). The truncated GFP–CPG2–N3 lacking the C-terminal F-actin association domain was significantly depleted by extraction (96.9 ± 0.6% before vs. 6.1 ± 1.4% after extraction; $P = 5.1 \times 10^{-39}$, Student *t* test), whereas the C5 fragment, featuring only the F-actin association domain, was not (89 ± 2.7% after extraction) (Fig. 2 *F* and *G*). These results demonstrate that CPG2 in neurons is physically anchored to the F-actin cytoskeleton in dendritic spines via its C-terminal F-actin association domain.

CPG2 Binding to F-Actin Is Attenuated by an Intramolecular Repressor Region. The isolated CPG2 F-actin association domain (fragment C5) cosediments with actin even after brief exposure to the filaments before ultracentrifugation. FL CPG2 is soluble under such stringent conditions and will cosediment with F-actin only

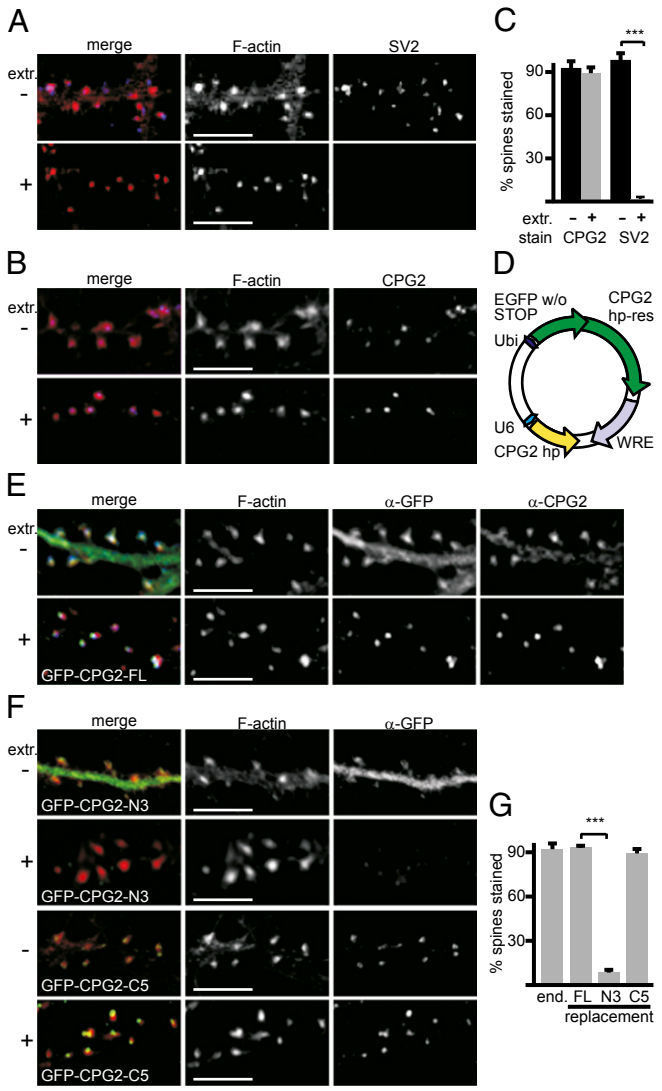

Fig. 2. Association with F-actin anchors CPG2 in dendritic spines. (*A*) Dendritic segments of cultured hippocampal neurons stained for F-actin and SV2. Neurons were either fixed without extraction (extr.) (–, *Upper*) or with extraction (+, *Lower*). (Scale bars: 10 μm.) (*B*) Neurons were treated as in *A* but immunostained for CPG2. (Scale bar: 7 μm.) (*C*) Quantification of percentage of spines staining positive for CPG2 or SV2 with or without extraction. CPG2, $n = 289$ extr., 302 without extr.; SV2, $n = 334$ extr., 323 without extr.; $^{***}P < 0.001$, Student t test. (*D*) Schematic of the lentiviral CPG2 replacement vector. Expression of EGFP is driven by the ubiquitin promoter. The stop codon of EGFP has been removed and an hp-resistant CPG2 is cloned in-frame to create EGFP–CPG2 fusion proteins. (*E*) Staining for F-actin, GFP, or CPG2 in cultured hippocampal neurons infected with FL CPG2 replacement virus (GFP–CPG2 FL) without extraction (*Upper*) or with extraction (*Lower*). (Scale bars: 10 μm.) (*F*) Neurons were infected with an hp-resistant CPG2–N3 or –C5 truncation fused to EGFP. –, without extraction; +, with extraction. (Scale bars: 7 μm.) (*G*) Quantification of percentage of immunostained spines with or without extraction for GFP–CPG2 FL, GFP–CPG2–N3 and GFP–CPG2–C5 compared with endogenous CPG2 (end.). $^{***}P < 0.001$, Student t test.

after prolonged exposure to polymerized filaments (Fig. 1*C*). Upon stringent, brief exposure FL CPG2 remains in the supernatant, as does a protein fragment containing 354 aa in addition to the C5 domain (CPG2-C6) (Fig. 3 *A* and *B*), suggesting that F-actin association is attenuated in the FL and CPG2-C6 proteins. To map the region repressing FL CPG2 actin association we generated chimeric constructs where parts of CPG2 were replaced with luciferase sequence (Fig. 3*A*). Chimeras with as few as 25 aa replaced directly upstream of the C5 fragment readily associated with F-actin under stringent conditions (constructs X3, X4, and X10, Fig. 3*A* and *C*), while those containing this region did not (FL, C6, X2, and C11). This data demonstrates that association with F-actin is repressed in FL CPG2 by a short stretch of 25 aa directly preceding the F-actin association domain.

CPG2 Binding to F-Actin in Vitro Is Positively Regulated by PKA Phosphorylation. Because in vivo the CPG2 internal repressor must somehow be counteracted to allow its association with F-actin, we tested whether kinases predicted to phosphorylate CPG2 could influence its F-actin association. Phosphorylation by the catalytic subunit of PKA significantly increased both FL CPG2 and CPG2–C6 association with F-actin under stringent conditions. (supernatant/pellet ratio 6.8 ± 0.9 and 7.4 ± 0.9, respectively, without PKA, vs. 2.3 ± 0.5 and 3.3 ± 0.8, respectively, with PKA; $P = 0.001$ and $P = 0.034$, respectively, Student t test) (Fig. 4 *A* and *B*), suggesting that PKA-mediated phosphorylation positively regulates CPG2 association with F-actin.

To map the PKA phosphorylation sites on CPG2, two overlapping fragments spanning the CPG2 coding region were expressed in bacteria as N-terminal GST fusions and subsequently purified (CPG2–N3 and CPG2–C6, shown in Fig. 4*C*; CPG2 FL did not express in sufficient amounts for purification.) Purified GST-fusion proteins were phosphorylated with various amounts of PKA for 20 min at 30 °C. Both GST–CPG2–N3 and GST–CPG2–C6 were phosphorylated by catalytic amounts of PKA (Fig. 4*D*). To detect high-specificity phosphorylation sites, we subjected the GST fusions to catalytic amounts of kinase for

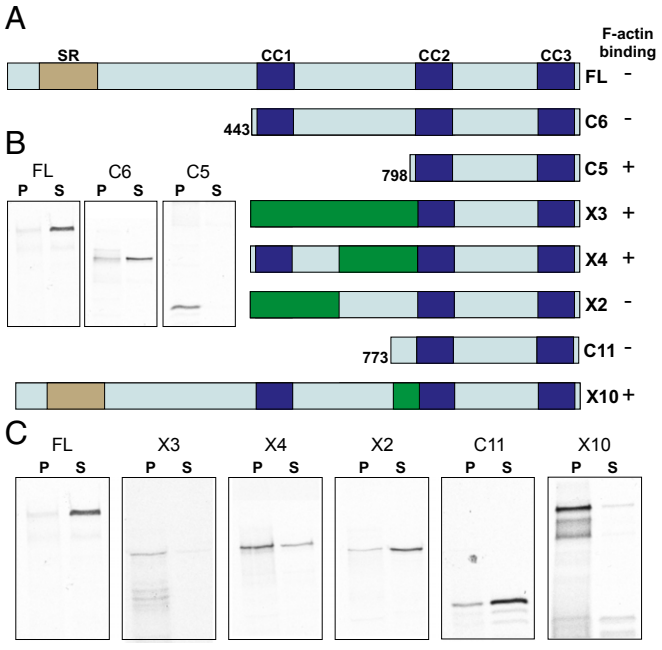

Fig. 3. Binding to F-actin is attenuated by protein sequence directly preceding the F-actin association domain. (*A*) Schematic of FL CPG2, as well as various truncations and chimeric constructs. Green parts denote unrelated protein sequence taken from the luciferase protein. (*B*) Representative autoradiography images for FL CPG2 and the C6 and C5 deletion constructs under stringent conditions for F-actin association. Note that the isolated F-actin association domain (C5) readily binds to F-actin under stringent conditions but FL CPG2 does not. (*C*) Various chimeric constructs reveal a short, 25-aa-long stretch that attenuates F-actin association in FL CPG2.

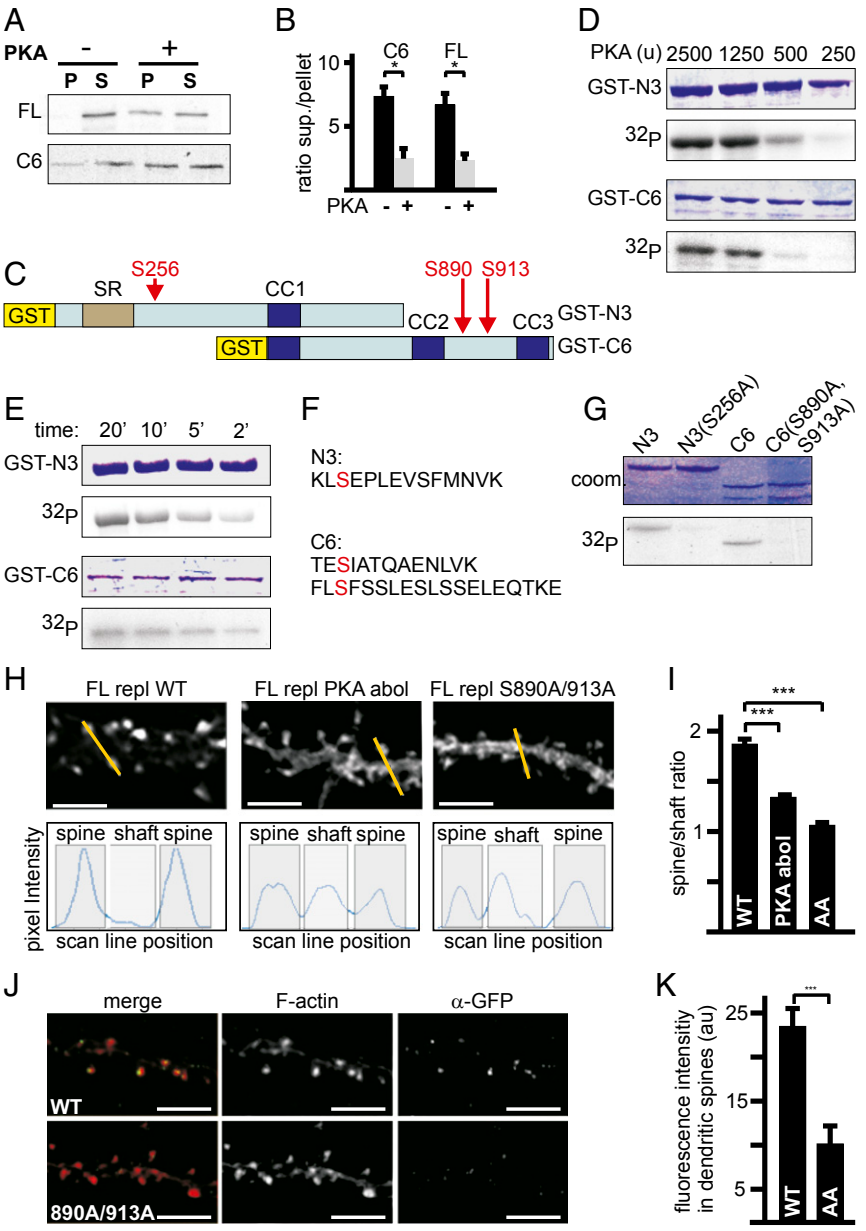

Fig. 4. PKA phosphorylates CPG2 in the F-actin association domain in vivo. (*A*) F-actin assay for FL CPG2 and CPG2–C6 under stringent conditions with (+) or without (–) phosphorylation by PKA. (*B*) Quantification of supernatant/pellet ratios showing increased F-actin pellet association of both FL CPG2 and CPG2–C6 in response to PKA phosphorylation. C6, $n = 8$, FL, $n = 7$; $^{*}P < 0.05$, Student t test. (*C*) Schematic of GST fusions to truncations N3 and C6, respectively. Sites in red denote high-specificity PKA phosphorylation sites. (*D*) Coomassie blue staining and autoradiography signals for PKA-phosphorylated GST–N3 (*Upper*) and GST-C6 (*Lower*), using indicated amounts of PKA for 20 min. (*E*) Time course of phosphorylation by 250 units PKA. (*F*) Peptides identified by mass spectrometry. Phosphorylated residues are shown in red and are depicted in *C*. (*G*) Coomassie blue staining and autoradiography signals of high-specificity PKA phosphorylation (250 units for 2 min) on GST–C6 and GST–N3, as well as mutant GST fusion proteins carrying phospho-incompetent alanine substitutions at the identified PKA target sites. (*H*) Representative images of dendritic segments from cultured hippocampal neurons expressing a GFP fusion to the indicated CPG2 WT or mutant cDNA and stained with anti-GFP. Line-scan analysis is shown for indicated trajectory through opposing spines. (Scale bars: 6 μm.) (*I*) Quantification of pixel intensities in spines vs. shafts for each mutant. $n = 804$ (WT), 1,258 (PKAabol), and 1,540 (AA), $^{***}P < 0.01$, Student t test. (*J*) Dendritic segments of cultured hippocampal neurons expressing a GFP fusion to either WT CPG2 or the S890A/S913A double mutant. Cells were extracted, fixed, and stained with rhodamine phalloidin (red) and anti-GFP (green). (Scale bars: 10 μm.) (*K*) Quantification of fluorescence intensity (arbitrary units) in F-actin–positive spine heads following extraction. $n = 288$ (WT) and 359 (AA); $^{***}P < 0.001$, Student t test.

various times and found that both fragments were phosphorylated by PKA within 2 min after incubation (Fig. 4*E*). These phosphorylated fusion proteins were submitted to mass spectrometry. Peptide analysis identified three peptides carrying a phosphate residue, with the phosphorylation sites mapping to S256, S890, and S913 within CPG2 FL (Fig. 4*F*, also marked in Fig. 4*C*). To assess whether these high-specificity PKA sites represent the complete ensemble of CPG2 PKA sites, we mutated the three identified serine residues to alanines, rendering them phospho-incompetent. The mutant GST-fusion proteins show virtually no PKA-mediated phosphorylation under high-specificity conditions (Fig. 4*G*). Thus, S256, S890, and S913 likely comprise the complete set of specific PKA phosphorylation sites within CPG2.

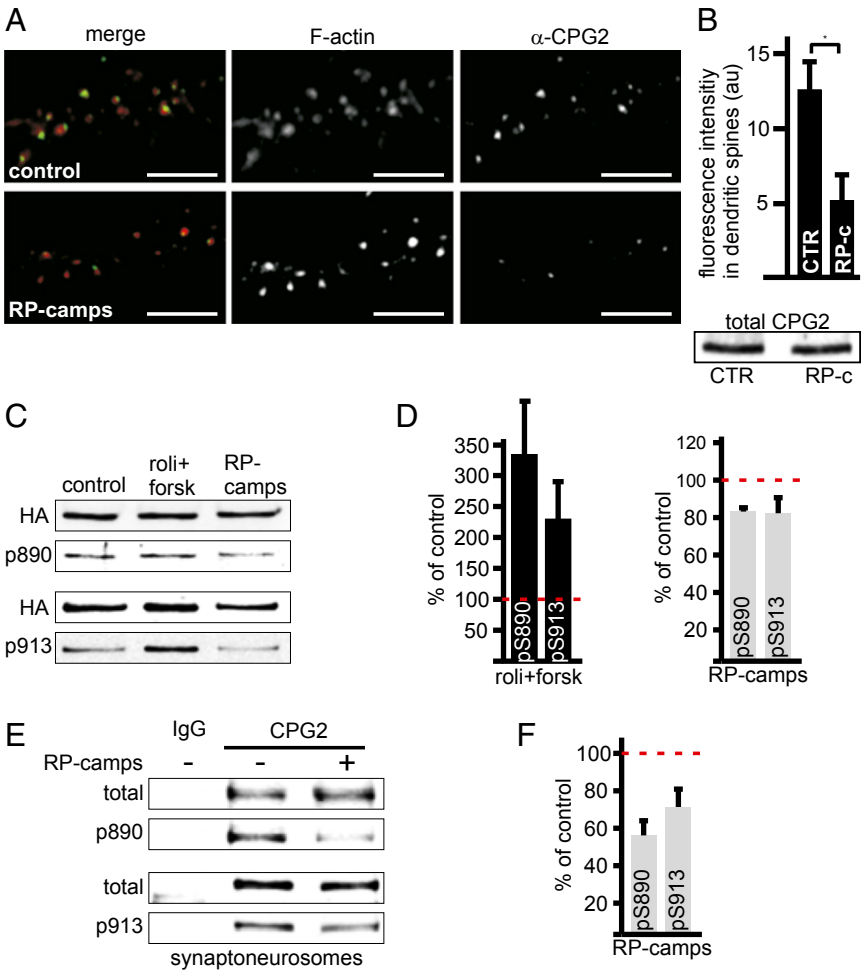

Fig. 5. PKA phosphorylation is required for actin binding in vivo. (*A*) Acute blockade of PKA signaling in cultured hippocampal neurons leads to significant reduction of endogenous CPG2 in dendritic spines. Cells were stained with rhodamine phalloidin (red) and anti-CPG2 (green). (Scale bars: 10 μm.) (*B*) Quantification of fluorescence intensity (arbitrary units, au) in F-actin-positive spine heads. n = 198 (control) and 229 (RP-camps); $^*P < 0.05$, Student t test. (*Lower*) Western blot showing total CPG2 levels under control conditions vs. RP-camps (RP-c). (*C*) Expression of HA–CPG2 in HEK293 cells and specific detection of phospho-S890 or phospho-S913 signals after stimulation of PKA with rolipram and forskolin (roli+forsk) or inhibition by RP-camps. (*D*) Quantification of S890 and S913 phospho-specific signal in response to rolipram and forskolin (roli+forsk, *Left*) or RP-camps (*Right*). (*E*) Synaptoneurosomes from rat brain, control (–) or subjected to PKA blockade by RP-camps (+), were probed for total CPG2 or phospho-S890 and S913. (*F*) Quantification of phospho-specific signals upon PKA blockade in synaptoneurosomes.

CPG2 Binding to F-Actin and Spine Localization in Vivo Are Positively Regulated by PKA Phosphorylation. To test whether the three CPG2 PKA phosphorylation sites mapped in vitro are required for CPG2 binding to F-actin in vivo, we used the viral replacement strategy to exchange endogenous CPG2 in cultured hippocampal neurons with either a GFP–FL CPG2 WT control or a GFP–FL CPG2 with all three PKA sites mutated to alanine residues (PKAabol). Anti-GFP antibody staining revealed that whereas the WT GFP–FL CPG2 protein was enriched in spine heads similar to endogenous CPG2 (Fig. 2*B*), the PKAabol ensemble mutant was not (Fig. 4*H*, *Left* and *Center*). Spine/shaft pixel intensity ratios were significantly different between WT GFP–FL CPG2 (1.83 ± 0.04) and PKAabol (1.32 ± 0.01, $P = 1.28 \times 10^{-61}$, Student t test) (Fig. 4*I*). Because the C6 construct lacking the S256 site was capable of binding to F-actin upon in vitro phosphorylation (Fig. 4 *A* and *B*), we speculated that the S256 site is not critical for CPG2 binding to F-actin. Indeed, a GFP–FL CPG2 mutant where only the two C-terminal PKA target sites are mutated showed reduced spine association similar to the PKAabol mutant (1.05 ± 0.001, $P = 2.01 \times 10^{-49}$, Student t test) (Fig. 4 *H* and *I*). Ablation of a single S256, S890, or S913 phosphorylation site did not affect spine enrichment (Fig. S3). These data suggest that either the S890 or the S913 PKA phosphorylation site on CPG2 is sufficient for its localization to dendritic spines. To confirm that PKA-mediated localization of CPG2 within dendritic spine heads is related to its cytoskeletal association, we tested whether the GFP–FL 890A/913A fusion protein could withstand mild Triton extraction. In contrast to WT GFP–FL CPG2, the phospho-incompetent double mutant GFP–FL 890A/913A showed significantly reduced association with F-actin in vivo (24.2 ± 2.4% for WT vs. 10.1 ± 2.4% for the S890A/S913A double mutant, $P = 2.2 \times 10^{-5}$, Student t test) (Fig. 4 *J* and *K*). Thus, PKA-mediated phosphorylation on either S890 or S913 is sufficient and required for CPG2 association with the cytoskeleton in dendritic spine heads and its enriched localization at this site.

PKA Phosphorylation of Endogenous CPG2 Is Required for Spine Localization and Actin Binding. To test whether spine localization of CPG2 in vivo is PKA-dependent we treated cultured neurons with the PKA blocker RP-camps. We found a significant decrease in endogenous CPG2 levels in dendritic spines after PKA

blockade despite unchanged total CPG2 levels (12.4 ± 2.3, n = 104 for control vs. 5.1 ± 1.7, n = 134 for RP-camps, P = 0.019, Student t test, Fig. 5 A and B). When HEK293 cells expressing HA-tagged CPG2 were probed with phospho-specific antibodies raised against phospho-S890 or phospho-S913, the phospho-specific signals for both sites were increased in response to rolipram and forskolin, which elevate cAMP levels and lead to increased PKA signaling (330 ± 86% for pS890; 227 ± 60% for pS913, normalized to HA signal intensity, Fig. 5 C and D). Blockade of endogenous PKA through RP-camps led to a decrease of normalized phospho-specific signals (83.4 ± 1.9% for pS890 and 82.8 ± 0.8% for pS913, Fig. 5 C and D). Likewise, treatment of synaptoneurosomes from adult rat brain with RP-camps led to a reduced phospho-specific signal at both sites (55.3 ± 7.5% for pS890; 70.6 ± 9.8% for pS913; Fig. 5 E and F). These data demonstrate that endogenous CPG2 is phosphorylated in vivo by PKA at both the S890 and S913 sites.

Phosphorylation of CPG2 by PKA Is Required for Functional Glutamate Receptor Endocytosis. We next investigated whether CPG2 phosphorylation by PKA was required for its function as a regulator of glutamate receptor endocytosis by combining the viral replacement strategy with a biotinylation assay to assess internalization of surface AMPARs. Consistent with other reports (15), we found that under basal conditions 11.1 ± 1.2% of GluA2 containing AMPARs are internalized within 30 min (Fig. 6A).

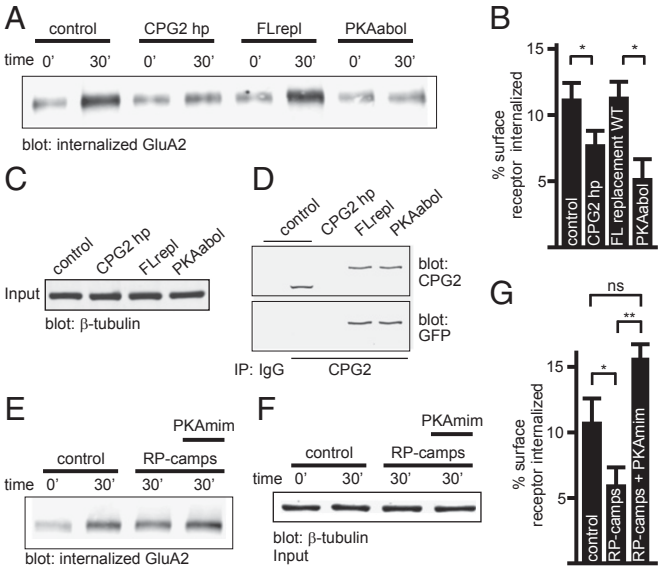

Fig. 6. PKA phosphorylation of CPG2 regulates glutamate receptor internalization. (*A*) Surface proteins of cultured cortical neurons infected with virus encoding either GFP (control), or the indicated CPG2 knockdown or replacement cassette, were labeled with a cleavable biotin tag. After 30 min at 37 °C remaining surface labels were stripped and internalized membrane proteins were affinity-purified. Representative Western blot for GluA2 is shown. (*B*) Quantification of internalized GluA2 after 30 min. Control, n = 20; CPG2hp, n = 22; FLreplace WT, n = 14; PKAabol, n = 19; *P < 0.05, Student t test. (*C*) Western blot of virally infected neurons shown in *A* probed for tubulin, showing equal input material for the internalization assay. (*D*) Western blots showing effective removal of endogenous CPG2 by shRNA knockdown, and expression of GFP fusions to FL replacement WT or the PKAabol mutant. (*E*) Acute blockade of PKA signaling with RP-camps leads to reduced GluA2 internalization. Introduction of a CPG2 phospho-mimetic S890E/S913E double mutant (PKAmim) overrides this effect. (*F*) Western blot of virally infected neurons shown in *E* probed for tubulin, showing equal input material for the internalization assay. (*G*) Quantification of the results from the experiment in *E*. Control, n = 16; RPcamps, n = 19; PKAmim, n = 5; *P < 0.05, Student t test.

Removal of CPG2 led to a significant decrease in glutamate receptor internalization (7.8 ± 1.2%, P = 0.032, Student t test, quantified in Fig. 6 B and C), consistent with our previous findings (11). Viral replacement of endogenous CPG2 with the CPG2 FL (Fig. 6D) rescued glutamate receptor internalization to normal values (11.2 ± 1.1%), but replacement with the CPG2 PKAabol mutant did not (5.1 ± 1.5%, P = 0.002; Student t test) (Fig. 6 A and B). We next investigated whether acute manipulation of PKA activity could affect glutamate receptor internalization and whether these effects were mediated through CPG2. PKA blockade by RP-camps in the internalization step led to a significant decrease in internalized GluA2 receptors, which was prevented in neurons expressing a phospho-mimetic S890E/S913E double-mutant CPG2 (Fig. 6 E–G; control 10.7 ± 1.8%, n = 16; RP-camps 5.9 ± 1.4%, n = 19; RP-camps with FLrepPKAmim 15.5 ± 1.1%, n = 5; control vs. RP-camps: P = 0.04; RP-camps vs. RP-camps with FLrepPKAmim: P = 0.006, control vs. RPcamps with FLrepPKAmim not significant: P = 0.22). The mimetic mutant alone displayed spine enrichment and actin binding comparable to WT CPG2 and was able to rescue receptor internalization to normal levels (Fig. S4). These data show that CPG2 phosphorylation at the two PKA sites essential for its association with F-actin is also required for normal levels of glutamate receptor endocytosis and that the effects of PKA on receptor internalization are mediated through CPG2.

CPG2 Knockdown Enhances Synaptic Strength in Vivo. To determine whether CPG2's role in glutamate receptor endocytosis is relevant to modulation of synaptic strength we used the viral-mediated knockdown and replacement strategy to manipulate CPG2 in neocortical pyramidal neurons and measured AMPAR miniature excitatory postsynaptic currents (mEPSCs).

To knock down CPG2 in vivo, viral injections were targeted to the primary visual cortex of 12- to 14-d-old rat pups, and slice recordings were performed 14 d later (at postnatal days 26–28) from layer-5 pyramidal neurons. Animals were injected with lentivirus carrying either an empty vector, one of the three hairpins directed against CPG2 (hp255, 1168, or 1897), or a hairpin along with a replacement FL CPG2 or CPG2 PKAabol mutant. Whole-cell mEPSC recordings revealed that CPG2 knockdown with two different hairpins significantly increased mEPSC amplitude relative to empty vector controls (Fig. 7A; P < 0.05) but had no significant impact on mEPSC frequency and kinetics, or on passive cell properties (Table S1). Changes in mEPSC amplitude could in theory arise from changes in AMPAR properties, but the lack of CPG2 knockdown effects on mEPSC kinetics suggests this is unlikely (16). However, the change in mEPSC amplitude is fully consistent with our culture data showing that loss of CPG2 enhances surface AMPAR accumulation and strongly suggests that this regulation extends to synaptic receptors (11).

Replacement with FL CPG2 rescued the increase in mEPSC amplitude caused by CPG2 knockdown (Fig. 7B, FL replacement not different from empty vector control, P = 0.98). In marked contrast, the CPG2 PKAabol mutant was unable to prevent the increase in mEPSC amplitude induced by endogenous CPG2 knockdown (Fig. 7B; PKAabol significantly different from empty vector control, P = 0.04). Taken together, these data demonstrate that CPG2 phosphorylation plays a role in the maintenance of postsynaptic strength at central glutamatergic synapses.

Discussion

Our data demonstrate a direct functional link between CME and the F-actin cytoskeleton that has implications for AMPAR endocytosis and the modulation of synaptic strength. Moreover, the regulation of CPG2/F-actin association by PKA provides a gateway for cellular control of synaptic receptor internalization through second messenger signaling pathways.

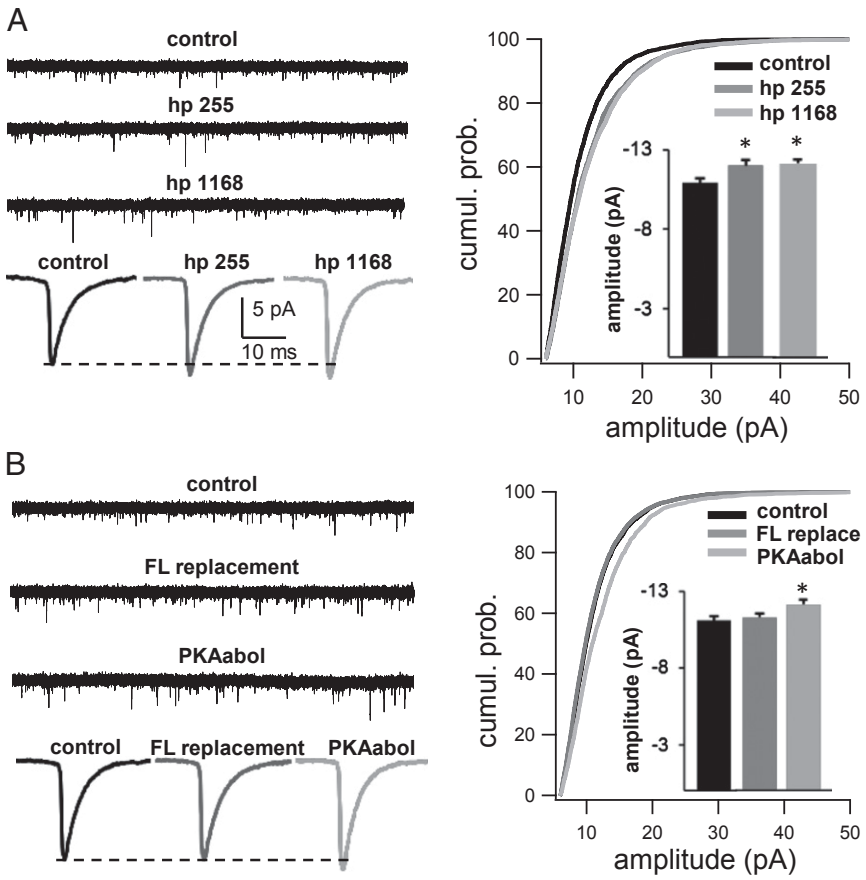

Fig. 7. CPG2 knockdown enhances synaptic strength in vivo. (*A*) (*Upper Left*) Examples of mEPSC recordings from empty vector control-, hp255- and hp1168-infected neurons in layer 5 of primary visual cortex. (*Lower Left*) Average mEPSC waveform for each condition. (*Right*) Cumulative distributions of mEPSC amplitudes for control, hp255 and hp1168. (*Inset*) Summary of mean mEPSC amplitude for each condition. (*B*) (*Upper Left*) Examples of mEPSC recordings from empty vector control-, FL replacement- and PKAabol-infected neurons. (*Lower Left*) Average mEPSC waveform for each condition. (*Right*) Cumulative distributions of mEPSC amplitudes for control, FL replacement and PKAabol. (*Inset*) Summary of mean mEPSC amplitude for each condition. Different from control, $*P < 0.05$.

Role of CPG2 in Linking F-Actin with the Endocytic Cycle. A dynamic F-actin cytoskeleton is known to be important for CME in yeast as well as in mammals. However, our understanding of how the endocytic process is mechanistically coupled to the cytoskeleton is vague. Various proteins have been suggested as linkers, for example HIP-1 (Huntingtin interacting protein 1) in combination with its close relative HIP1-R. HIP-1 binds to clathrin, whereas HIP-1R associates with F-actin. Formation of HIP-1 and HIP-1R heterodimers may bridge the endocytic machinery and F-actin filaments (reviewed in ref. 17). Dynamins, too, have several indirect points of contact with the actin cytoskeleton through Profilin (18), Cortactin (19), Abp-1 (20), and Intersectin (17). However, the regulation of these interactions and their functional significance to CME remain unclear.

Because CPG2 directly links CME to the cytoskeleton, the consequence of CPG2 knockdown provides insight into the mechanistic role of the cytoskeleton in CME. In the absence of CPG2, clathrin-coated vesicles accumulate in the postsynaptic compartment (11), suggesting that CME coupling to the cytoskeleton is required for vesicle uncoating. Loss of Synaptojanin, a protein known to promote endocytic vesicle uncoating, like loss of CPG2, also leads to increased AMPAR surface expression as well as impaired constitutive and NMDA-induced internalization of AMPARs (21). Actin polymerization may help propel newly endocytosed vesicles into the spine cytosol where the activity or local concentration of uncoating proteins such as Synaptojanin is potentially higher. CPG2 may facilitate this process by attaching newly endocytosed vesicles to F-actin filaments at the plasma membrane.

Relationship Between CPG2, Endocytic Machinery, and Synaptic Plasticity. Targeted disruption of endocytic factors has revealed their importance for synapse physiology at both presynaptic (22–24) and postsynaptic sites (25). Our data show that reducing CPG2 levels or replacing it with a phospho-incompetent mutant (PKAabol) reduces AMPAR endocytosis and enhances surface AMPAR levels and AMPA quantal amplitude. This is consistent with previous studies in which manipulations of proteins that interact with the AMPAR endocytic machinery were shown to perturb the steady-state number of AMPAR at synaptic sites (26). CPG2 function may have particular significance in the context of synaptic plasticity, because regulated AMPAR internalization plays a critical role in several forms of synaptic plasticity, including LTD (27, 28) and homeostatic synaptic down-scaling (29).

Reducing CPG2 levels reduces, but does not abolish, AMPAR endocytosis. Because CPG2 knockdown is not complete (85–90%), the fraction of remaining molecules may be sufficient to facilitate the low-level AMPAR internalization we observe. Alternatively, CPG2-independent pathways for retrieving AMPARs from the cell membrane may exist. A more interesting possibility is that CPG2 function is not strictly necessary for basal AMPAR CME, but that the CPG2/F-actin interaction enhances the efficiency of AMPAR endocytosis in response to externally activated signaling pathways. Knockdown of CPG2 enhances

quantal amplitude by ~10%. Changes of this magnitude in basal mEPSC amplitude are within the range observed for manipulations of other proteins important for AMPAR trafficking (30, 31). The effect of CPG2 knock down on total surface AMPAR accumulation (~20% enhancement) is larger than that on mEPSC amplitude. This is unlikely to be due to differences in the sensitivity of the assays, because mEPSC recordings are a very sensitive read-out of changes in synaptic receptor accumulation and unlikely to dramatically underestimate a change in synaptic receptor abundance (32). One possible explanation is that, whereas extrasynaptic AMPAR abundance is regulated mostly through endo- and exocytosis, the synaptic accumulation of AMPAR is also strongly influenced by scaffold proteins that tether receptors at synapses. Consequently, the effects of increasing total surface AMPAR on synaptic abundance could be sublinear if available scaffold binding sites are limiting. Interestingly, homeostatic forms of synaptic plasticity that involve changes in AMPAR endocytosis also lead to changes in synaptic scaffolds (33), suggesting that during some forms of synaptic plasticity these two factors that regulate synaptic AMPA abundance may be regulated in parallel to efficiently change synaptic strength.

CPG2 As a Mediator of PKA Signaling in Synaptic Plasticity. A genome-wide functional analysis of all known kinases identified the cAMP/PKA pathway as an activator of CME (34). In the context of neurons, PKA has been reported to phosphorylate the GluA1 subunit of AMPARs, delivering GluA1-containing receptors to extrasynaptic sites on the cell surface. Synaptic incorporation requires concomitant phosphorylation by CamKII, and both phosphorylation events together are critical for LTP expression (reviewed in ref. 35). cAMP analogs prevent hippocampal LTD, and PKA inhibitors produce synaptic depression that occludes LTD (36). Conversely, PKA has also been shown to positively regulate LTD. Knock-in mice expressing a mutant A-kinase anchoring protein 150 (AKAP150) deficient in PKA binding show a 90% reduction in hippocampal LTD (37). These latter observations are consistent with our findings that PKA phosphorylation of CPG2 is required for functional AMPAR endocytosis. However, other scenarios are also possible. An instructive role for PKA in AMPAR endocytosis, via CPG2, could play out on a different time scale from GluA1 phosphorylation and may serve to counteract an overshoot of AMPAR synaptic delivery. Alternatively, PKA phosphorylation of CPG2 and GluA1 may occur in response to different upstream signaling events that activate PKA through segregated channels. Timing of PKA activation in combination with its localization in dendritic spine heads vs. shafts could potentially influence downstream effects on AMPAR cycling. It is also possible that PKA activation in the absence of CamKII signaling may favor LTD, but concomitant PKA and CamKII signaling negate the facilitation of endocytosis by CPG2, thus favoring LTP.

Summary

In summary, our data show that CPG2 regulates synaptic AMPAR endocytosis through its association with the spine cytoskeleton and functions as a nexus for integrating PKA signaling with this process. We are not aware of other proteins that act to integrate second messenger signaling with CME coupling to the actin cytoskeleton. Because the *Cpg2* message is restricted to brain tissue (11) and the CPG2 protein is specifically localized to excitatory synapses onto excitatory neurons, we suggest that CPG2 is not a canonical component of the endocytic machinery. We speculate that in nonneuronal cells other proteins could act as nexus molecules that integrate second messenger signaling and reversibly associate with the cytoskeleton to commandeer the endocytic process, analogous to the role of CPG2.

Materials and Methods

In Vitro Transcription/Translation and F-Actin Association. In vitro transcription/translation (TNT; Promega) was carried out according to the manufacturer's instructions. In brief, pcDNA3-CPG2 was incubated with the TNT mix and [^{35}S]methionine (Perkin–Elmer) for 90 min at 30 °C. Radiolabeled proteins were then purified by immunoprecipitation, washed, and eluted with free HA peptide. Eluted proteins were incubated with polymerizing rabbit muscle actin (Sigma) for 25 min or 5 min. F-actin filaments were collected by ultracentrifugation at 100,000 × *g*. Supernatant and pellet fractions were run on SDS/PAGE, gels were dried between cellophane sheets, and Kodak Biomax MR film was exposed for 24 h.

Cloning and General Molecular Biological Techniques. Full-length *Cpg2* cDNA and truncations were inserted into pcDNA3-HA or pGEX-5X1 by restriction cloning. Site-directed mutagenesis was performed by the Kunkel method. Ensemble mutants were obtained through successive mutagenesis and the fidelity of all constructs was confirmed by sequencing (Retrogen). Lentiviral vectors were based on pFUGW (38). The EGFP stop codon was removed and a multiple cloning site was inserted. CPG2 hairpin (hp) cassettes were introduced into the PacI site by amplification of the hp and upstream U6 promoter from pSilencer. Lentiviral particles were generated in HEK cells using described techniques (39) and titers of 5×10^5 to 5×10^6 cfu/μL were routinely obtained.

Phosphorylation Assays and Mass Spectrometry. GST fusion proteins were expressed from pGEX-5X1 (Amersham) in Rosetta2 cells upon induction with 1 mM IPTG. Eight hours postinduction, cells were collected and lysed by sonication. Proteins were precipitated using immobilized glutathione (Pierce), eluted with 25 mM free reduced glutathione (Cayman), and dialyzed in 20 mM Tris, pH 7.9 overnight. Purified protein was phosphorylated by PKA (New England Biolabs) according to the manufacturer's instructions at 30 °C for indicated times in the presence of [γ-^{32}P]ATP (Perkin–Elmer). Protein samples were separated by SDS/PAGE, stained with Coomassie brilliant blue, dried, and film was exposed for 24 or 48 h. For site identification, phosphorylation was done under high-specificity conditions, without radioactivity. Samples were excised from SDS gels and analyzed for phosphopeptides after tryptic digestion at the Taplin Mass Spectrometry facility (Harvard University).

Immunocytochemistry Quantifications. Data were quantified using ImageJ. Intensity values from line-scan analysis were graphically depicted using Microsoft Excel. Ratios for synaptic enrichment were quantified by measuring pixel intensities within spine heads vs. a selection of dendritic shaft of the same size and located directly beneath the corresponding spine neck. For extraction assays, individual spine heads were defined as regions of interest (ROIs) using the red channel (phalloidine). Staining intensity of the GFP–CPG2 fusion proteins was subsequently measured for each ROI in the corresponding green channel (anti-GFP signal).

Pharmacology. RP-camps (5 μM), rolipram (10 μm), and forskolin (5 μM) (all from Tocris) or control solvent were applied to the media for 30 min where indicated.

In Vivo Lentivirus Delivery. Lentivirus injections were performed on 12- to 14-d-old Long Evans rat pups. Rats were anesthetized by an i.p. injection of ketamine (70 mg/kg), xylazine hydrochloride (3.5 mg/kg), and acepromazine maleate (0.7 mg/kg) mixture and placed in a stereotaxic frame. Coordinates of the injection site into monocular region of the visual cortex (V1M) were determined using ref. 40 and adjusted for the brain size difference (2.5 mm lateral and 0.8 mm caudal from lambda). A total volume of 2 μL of lentivirus suspension was injected through a glass micropipette using a Starrett microinjector (model 762). Viral titers varied between 2–8 × 10^6 cfu/μL and were injected bilaterally to provide within-animal control: Empty vector control was injected in the right brain hemisphere with CPG2 hairpin-containing virus (hp255 or hp1168) in the left, and full-length CPG2 replacement virus (FL replacement, right hemisphere) with PKA phosphorylation-lacking mutant (PKAabol, left hemisphere). Animals were left to recover for 14 d before proceeding with electrophysiological experiments.

Electrophysiology. Visual coronal brain slices and mEPSC recordings were performed and analyzed as previously described (41). Coronal slices containing primary visual cortex were prepared from virus injected, 26- to 28-d-old rats. Animals were deeply anesthetized with isoflurane and decapitated. Brains were quickly removed and placed in chilled oxygenated (95% O_2 and 5% CO_2) artificial cerebrospinal fluid (ACSF) containing 126 mM NaCl, 3 mM KCl, 2 mM $MgSO_4$, 1 mM NaH_2PO_4, 26 mM $NaHCO_3$, 2 mM $CaCl_2$, and 20 mM

dextrose. Slices of 300-μm thickness were cut on a Leica VT100S vibratome and incubated at 35 °C for 30 min before use. For recording, slices were transferred to a submerged chamber mounted on a fixed-stage upright microscope and continuously perfused with warmed (37 °C) oxygenated ACSF. Patch-clamp recordings were obtained from layer V in the monocular region of V1 using a Multiclamp 700B amplifier. Virus infected pyramidal neurons were identified based on their expression of GFP and patched with glass micropipettes (3- to 5-MΩ resistance) filled with 100 mM K-gluconate, 20 mM KCl, 10 mM K-Hepes, 0.3 mM Na-GTP, 4 mM Mg-ATP, 10 mM Na-phosphocreatine, and 0.1% biocytin (pH 7.35). Post hoc staining and morphological reconstruction of biocytin-filled cells was used for neuron classification, in addition to their firing and synaptic properties. Recordings were discarded if the membrane resting potential was more positive than −60 mV, series resistance larger than 25 MΩ, resting input resistance smaller than 50 MΩ, or if any of these properties changed by more than 10% during the course of the recording. To isolate AMPA-mediated mEPSCs, neurons were held in voltage clamp at −70 mV in the presence of 1 μM TTX, 50 μM 2-amino-5-phosphono-valeric acid, and 20 μM picrotoxin. In-house software was used to detect and measure mEPSCs. Detection criteria included amplitude greater than 5 pA and 20–80% rise time less than 1 ms. All data are expressed as mean ± SEM, unless otherwise noted. Unpaired Student *t* tests were used for statistical analyses of individual hp data compared with the matched empty vector controls (recordings from left vs. right hemisphere). For multiple comparisons ANOVA was followed by a Dunnett test. A *P* value equal to or smaller than 0.05 was considered statistically significant. There was no significant difference between any of the empty vector controls and FL replacement (ANOVA, *P* value 0.528). FL replacement and PKAabol data were compared with combined empty vector control data from all recordings (total control) by using a Dunnett test (total control vs. FL replacement, *P* value 0.983; total control vs. PKAabol, *P* value 0.036).

ACKNOWLEDGMENTS. We thank Emily Hager and Alexandra May for excellent technical support and members of the E.N. laboratory for critical reading of the manuscript. This work was supported by funding from the Picower Institute Innovation Fund and the Stanley Center for Psychiatric Research (E.N.), National Institutes of Health Grant NS036853 (to G.G.T.), and Scholarship LO 1455/1-1 from the Deutsche Forschungsgemeinschaft (to S.L.).

1. Doherty GJ, McMahon HT (2009) Mechanisms of endocytosis. *Annu Rev Biochem* 78: 857–902.
2. Qualmann B, Kessels MM, Kelly RB (2000) Molecular links between endocytosis and the actin cytoskeleton. *J Cell Biol* 150(5):F111–F116.
3. Liu J, Sun Y, Oster GF, Drubin DG (2010) Mechanochemical crosstalk during endocytic vesicle formation. *Curr Opin Cell Biol* 22(1):36–43.
4. Man HY, et al. (2000) Regulation of AMPA receptor-mediated synaptic transmission by clathrin-dependent receptor internalization. *Neuron* 25(3):649–662.
5. Wang YT, Linden DJ (2000) Expression of cerebellar long-term depression requires postsynaptic clathrin-mediated endocytosis. *Neuron* 25(3):635–647.
6. Shi S, Hayashi Y, Esteban JA, Malinow R (2001) Subunit-specific rules governing AMPA receptor trafficking to synapses in hippocampal pyramidal neurons. *Cell* 105(3): 331–343.
7. Holman D, Feligioni M, Henley JM (2007) Differential redistribution of native AMPA receptor complexes following LTD induction in acute hippocampal slices. *Neuropharmacology* 52(1):92–99.
8. Park M, Penick EC, Edwards JG, Kauer JA, Ehlers MD (2004) Recycling endosomes supply AMPA receptors for LTP. *Science* 305(5692):1972–1975.
9. Nedivi E, Hevroni D, Naot D, Israeli D, Citri Y (1993) Numerous candidate plasticity-related genes revealed by differential cDNA cloning. *Nature* 363(6431):718–722.
10. Nedivi E, Fieldust S, Theill LE, Hevron D (1996) A set of genes expressed in response to light in the adult cerebral cortex and regulated during development. *Proc Natl Acad Sci USA* 93(5):2048–2053.
11. Cottrell JR, Borok E, Horvath TL, Nedivi E (2004) CPG2: A brain- and synapse-specific protein that regulates the endocytosis of glutamate receptors. *Neuron* 44(4):677–690.
12. Hartwig JH (1994) Actin-binding proteins 1: Spectrin superfamily. *Protein Profile* 1(7): 706–778.
13. Loebrich S, Bähring R, Katsuno T, Tsukita S, Kneussel M (2006) Activated radixin is essential for GABAA receptor alpha5 subunit anchoring at the actin cytoskeleton. *EMBO J* 25(5):987–999.
14. Xu W, et al. (2008) Molecular dissociation of the role of PSD-95 in regulating synaptic strength and LTD. *Neuron* 57(2):248–262.
15. Ehlers MD (2000) Reinsertion or degradation of AMPA receptors determined by activity-dependent endocytic sorting. *Neuron* 28(2):511–525.
16. Thiagarajan TC, Lindskog M, Tsien RW (2005) Adaptation to synaptic inactivity in hippocampal neurons. *Neuron* 47(5):725–737.
17. McPherson PS (2002) The endocytic machinery at an interface with the actin cytoskeleton: A dynamic, hip intersection. *Trends Cell Biol* 12(7):312–315.
18. Witke W, et al. (1998) In mouse brain profilin I and profilin II associate with regulators of the endocytic pathway and actin assembly. *EMBO J* 17(4):967–976.
19. McNiven MA, et al. (2000) Regulated interactions between dynamin and the actin-binding protein cortactin modulate cell shape. *J Cell Biol* 151(1):187–198.
20. Kessels MM, Engqvist-Goldstein AE, Drubin DG, Qualmann B (2001) Mammalian Abp1, a signal-responsive F-actin-binding protein, links the actin cytoskeleton to endocytosis via the GTPase dynamin. *J Cell Biol* 153(2):351–366.
21. Gong LW, De Camilli P (2008) Regulation of postsynaptic AMPA responses by synaptojanin 1. *Proc Natl Acad Sci USA* 105(45):17561–17566.
22. Di Paolo G, et al. (2002) Decreased synaptic vesicle recycling efficiency and cognitive deficits in amphiphysin 1 knockout mice. *Neuron* 33(5):789–804.
23. Lou X, et al. (2012) Reduced release probability prevents vesicle depletion and transmission failure at dynamin mutant synapses. *Proc Natl Acad Sci USA* 109(8): E515–E523.
24. Zhang B, et al. (1998) Synaptic vesicle size and number are regulated by a clathrin adaptor protein required for endocytosis. *Neuron* 21(6):1465–1475.
25. Metzler M, et al. (2003) Disruption of the endocytic protein HIP1 results in neurological deficits and decreased AMPA receptor trafficking. *EMBO J* 22(13):3254–3266.
26. Rial Verde EM, Lee-Osbourne J, Worley PF, Malinow R, Cline HT (2006) Increased expression of the immediate-early gene arc/arg3.1 reduces AMPA receptor-mediated synaptic transmission. *Neuron* 52(3):461–474.
27. Malenka RC (2003) Synaptic plasticity and AMPA receptor trafficking. *Ann N Y Acad Sci* 1003:1–11.
28. Linden DJ (2012) A late phase of LTD in cultured cerebellar Purkinje cells requires persistent dynamin-mediated endocytosis. *J Neurophysiol* 107(1):448–454.
29. Evers DM, et al. (2010) Plk2 attachment to NSF induces homeostatic removal of GluA2 during chronic overexcitation. *Nat Neurosci* 13(10):1199–1207.
30. Ehrlich I, Malinow R (2004) Postsynaptic density 95 controls AMPA receptor incorporation during long-term potentiation and experience-driven synaptic plasticity. *J Neurosci* 24(4):916–927.
31. Soden ME, Chen L (2010) Fragile X protein FMRP is required for homeostatic plasticity and regulation of synaptic strength by retinoic acid. *J Neurosci* 30(50):16910–16921.
32. Umemiya M, Senda M, Murphy TH (1999) Behaviour of NMDA and AMPA receptor-mediated miniature EPSCs at rat cortical neuron synapses identified by calcium imaging. *J Physiol* 521(Pt 1):113–122.
33. Sun Q, Turrigiano GG (2011) PSD-95 and PSD-93 play critical but distinct roles in synaptic scaling up and down. *J Neurosci* 31(18):6800–6808.
34. Pelkmans L, et al. (2005) Genome-wide analysis of human kinases in clathrin- and caveolae/raft-mediated endocytosis. *Nature* 436(7047):78–86.
35. Gomes AR, Correia SS, Carvalho AL, Duarte CB (2003) Regulation of AMPA receptor activity, synaptic targeting and recycling: Role in synaptic plasticity. *Neurochem Res* 28(10):1459–1473.
36. Kameyama K, Lee HK, Bear MF, Huganir RL (1998) Involvement of a postsynaptic protein kinase A substrate in the expression of homosynaptic long-term depression. *Neuron* 21(5):1163–1175.
37. Lu Y, et al. (2008) AKAP150-anchored PKA activity is important for LTD during its induction phase. *J Physiol* 586(Pt 17):4155–4164.
38. Lois C, Hong EJ, Pease S, Brown EJ, Baltimore D (2002) Germline transmission and tissue-specific expression of transgenes delivered by lentiviral vectors. *Science* 295(5556):868–872.
39. Coleman JE, et al. (2003) Efficient large-scale production and concentration of HIV-1-based lentiviral vectors for use in vivo. *Physiol Genomics* 12(3):221–228.
40. Paxinos G, Watson C (1998) *The Rat Brain in Steriotaxic Coordinates* (Academic, San Diego), 4th Ed.
41. Maffei A, Turrigiano GG (2008) Multiple modes of network homeostasis in visual cortical layer 2/3. *J Neurosci* 28(17):4377–4384.

Supporting Information

Loebrich et al. 10.1073/pnas.1318860110

SI Materials and Methods

Neuron Cultures. Hippocampal and cortical neurons were derived from E18 Sprague–Dawley rat embryonic brains and plated at 3×10^4, 2×10^6, or 10×10^6 cells per 12-mm glass coverslip, 10-cm or 15-cm dish, respectively. Coverslips and dishes were precoated with poly-L-lysine. Cells were plated in NeuroBasal media containing 10% (vol/vol) FCS, GlutaMAX (Invitrogen), and B27 Supplement (Invitrogen). Media was exchanged to serum-free media 24 h after plating. At 8 d in vitro arabinofuranosylcytosine was added to 1 μM to prevent glial overgrowth. Cultures were kept at 37 °C and 5% CO_2 for 21 d.

Immunocytochemistry. Neurons were fixed in 4% (wt/vol) paraformaldehyde (PFA) solution for 12 min, permeabilized for 4 min in 0.25% Triton, blocked with 1% BSA, and primary antibodies were applied for 2 h at room temperature: α-candidate plasticity gene 2 (CPG2), mouse monoclonal, clone A6, 1:500; α-postsynaptic density-95 (PSD95) (1:300; Zymed); and α-GFP (1:3,000; Abcam). Rhodamine phalloidin was added with secondary antibodies for 45 min at room temperature: α-mouse 544, α-rabbit 488, or α-rabbit 663 (all AlexaFluor, 1:1,000). Extraction assays were performed by washing live neurons with ice-cold PBS then extracting cells on ice with ice-cold 0.5% Triton in PBS for 2 min followed by immediate fixation in PFA.

Quantifications of CPG2 Knockdown by Western Blotting. Ten-centimeter dishes of cortical neurons were infected with CPG2 hairpin (hp) virus at day 6 in vitro and scraped in homogenization buffer [150 mM NaCl, 50m M Tris (pH 7.6), and 0.5% Nonidet P-40]. Protein concentration was measured by BCA assay (Pierce) and 1 mg of total protein was offered to agarose beads conjugated with 5 μg of α-CPG2 antibody (clone A6). Samples were washed extensively, boiled, and separated by SDS/PAGE. CPG2 band intensities were measured using ImageJ.

Internalization Assay. Internalization assays were as previously described (1), with the following modifications: Ten-centimeter dishes of cortical neurons were infected with CPG2 hp virus at day 6 in vitro and subsequently with CPG2 replacement virus at day 18 in vitro. Blots were probed with anti-GluA2 antibody (1:2,000; Chemicon) and analyzed in an Odyssey infrared scanner (Licor).

1. Cottrell JR, Borok E, Horvath TL, Nedivi E (2004) CPG2: A brain- and synapse-specific protein that regulates the endocytosis of glutamate receptors. *Neuron* 44(4):677–690.

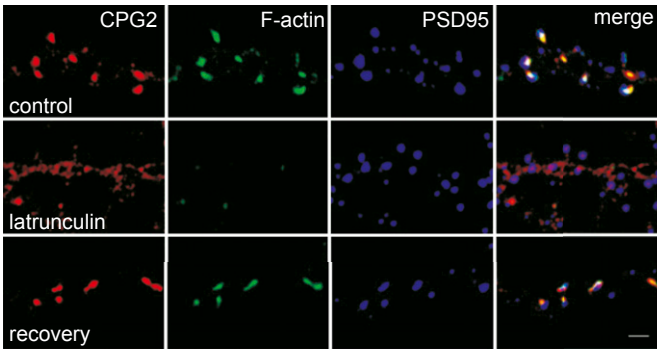

Fig. S1. CPG2 spine localization depends on F-actin. Cultured hippocampal neurons were untreated (control), treated with the F-actin depolymerizing agent latrunculin A, or treated with latrunculin A followed by a recovery period. Cultures were triple-labeled for CPG2, PSD-95, and F-actin. (Scale bar: 2 mm.)

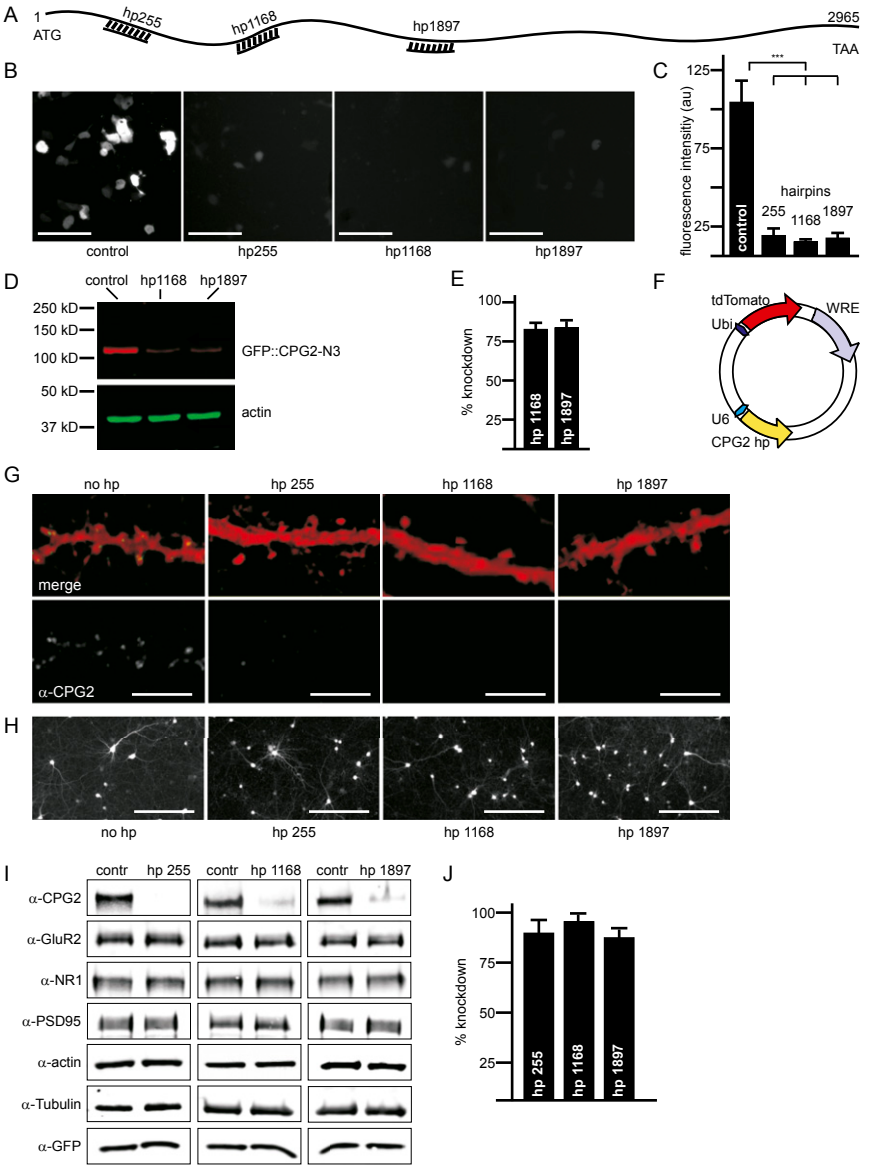

Fig. S2. Effective knockdown of CPG2 with three independent hps. (*A*) Schematic overview of CPG2 ORF and relative positions of the three hairpins hp255, hp1168, and hp1897. Start and stop codons are indicated. Numbers refer to nucleotide position in the ORF. (*B*) Immunocytochemistry using an anti-GFP antibody (Abcam) on cultured HEK cells transfected with a fusion cDNA of GFP::CPG2–N3 together with a pSilencer2.1 construct expressing either a random hp (control) or hp255, hp1168, or hp1897. (Scale bars: 200 μm.) (*C*) Quantification of fluorescence intensity in HEK cells by analysis of total pixel intensity within circular selections. ***$P < 0.01$, Student *t* test. (*D*) Western blot showing effective removal of the GFP::CPG2–N3 fusion protein in HEK cell lysates. (*E*) Quantification of knockdown efficiency in HEK cells by Western blotting. (*F*) Schematic of the lentiviral CPG2 hp vector. A small-hp RNA is driven by the U6 promoter, the red fluorescent tdTomato protein by the ubiquitin promoter (Ubi). WRE, woodchuck regulatory element. Analogous vectors were cloned using GFP instead of TdTomato. (*G*) Immunostaining for CPG2 protein on cultured hippocampal neurons infected with a virus expressing tdTomato and either containing no hp or one of the three hps specific for CPG2 (hp255, hp1168, or hp1897). (Scale bars: 10 μm.) (*H*) Representative images of cultured cortical neurons expressing GFP or tdTomato and the respective CPG2 hp cassette. (Scale bars: 500 μm.) (*I*) Western blot analyses of immunoreactivity for CPG2 as well as major synaptic components after CPG2 knockdown. Left lanes, a control lentivirus without hairpin expression cassette was used; right lanes, the indicated CPG2 knockdown hp was used. (*J*) Quantification of knockdown efficiency in neurons by Western blotting.

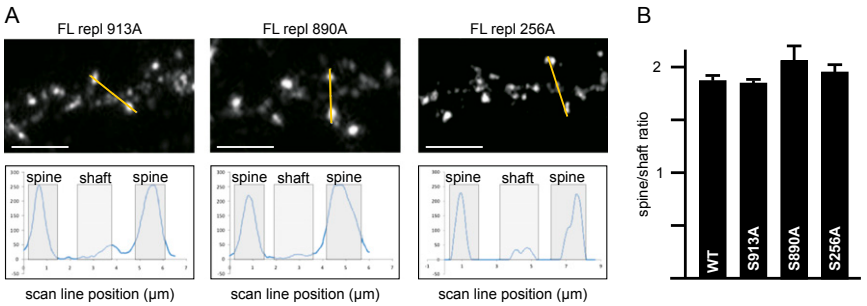

Fig. S3. Single mutants of PKA target sites are indistinguishable from WT CPG2. (*A*) Representative images of dendritic segments from cultured hippocampal neurons expressing a GFP fusion to the indicated CPG2 WT or mutant cDNA. Cells were fixed and stained with anti-GFP. Line-scan analysis is shown for indicated trajectory through opposing spines. (Scale bars: 6 μm.) (*B*) Quantification of pixel intensities in spines vs. shafts for each mutant. $n = 804$ (WT), 724 (S913A), 578 (S890A), and 687 (S256A). Spine/shaft ratios for the GFP–FL 256A, GFP–FL 913A, and GFP–FL 90A single mutants not significantly different from the WT protein (1.91± 0.07 for S256A; 1.82 ± 0.03 for S913A; 2.08 ± 0.08 for S890A; $P = 0.67$, $P = 0.88$, and $P = 0.25$, respectively, Student *t* test).

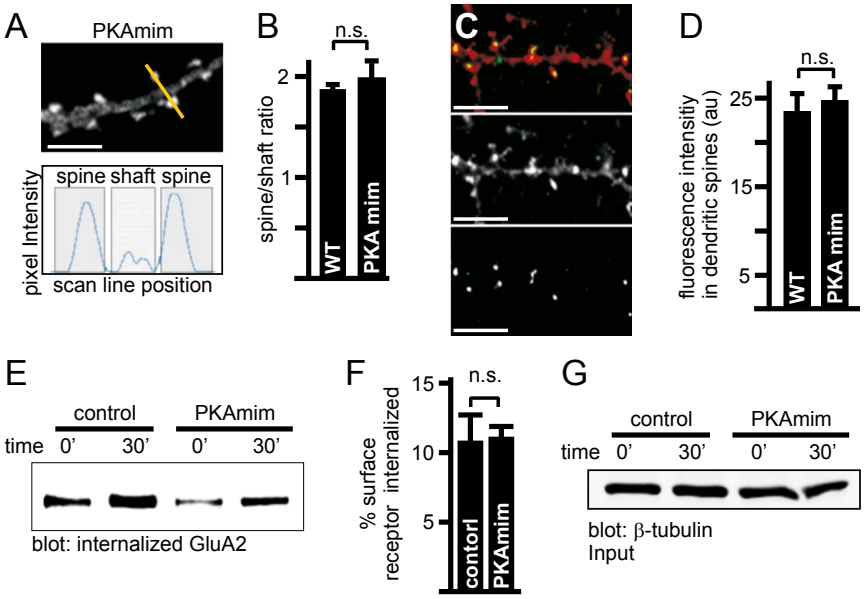

Fig. S4. The PKA phosphomimetic double mutant shows properties similar to WT CPG2. (*A*) Representative image of a dendritic segment from cultured hippocampal neurons expressing a GFP fusion to the S890E/S913E double mutant. Line-scan analysis is shown for indicated trajectory through opposing spines. (Scale bar: 6 μm.) (*B*) Quantification of pixel intensities in spines vs. shafts. $n = 1{,}138$ (WT) and 1,406 (PKAmim); 1.83 ± 0.04 for WT; 1.95 ± 0.15 for S890E/S913E $P = 0.41$, Student *t* test). (*C*) Dendritic segments of cultured hippocampal neurons expressing a GFP fusion to the S890E/S913E double mutant. Cells were extracted, fixed, and stained with rhodamine phalloidin (red) and anti-GFP (green). (Scale bars: 10 μm.) (*D*) Quantification of fluorescence intensity (arbitrary units) in F-actin–positive spine heads following extraction. $n = 288$ (WT) and 196 (PKAmim); 24.2 ± 2.4% for WT vs. 24.8 ± 1.8% for S890E/S913E; $P = 0.45$, Student *t* test. (*E*) Internalization rate of biotin-labeled glutamate receptors after replacement of endogenous CPG2 with the PKA phosphomimetic mutant (PKAmim) is comparable to control. Representative Western blot for GluA2 is shown. (*F*) Quantification of internalized GluA2 after 30 min: 10.7% ± 1.8 (control), 11.0% ± 0.8; control, $n = 20$; PKAmim, $n = 6$; $P = 0.45$, Student *t* test. (*G*) Western blot probed for tubulin showing equal input material.

Table S1. Parameters for electrophysiological recordings

Parameter	Control*	hp255	Control†	hp1168	Control‡	hp1897	WT repla.	PKAabol
Vm, mV	−67.4 ± 0.8	−66.5 ± 0.7	−67.1 ± 1.2	−67.1 ± 0.7	−66.4 ± 0.8	−66.5 ± 0.7	−67.3 ± 0.9	−70.2 ± 1.1
Rm, MΩ	113.4 ± 15.3	126.0 ± 23.4	114.2 ± 14.5	126.5 ± 21.6	113.3 ± 15.2	126.0 ± 23.4	131.1 ± 18.7	147.8 ± 22.8
Rise time, ms	0.58 ± 0.01	0.57 ± 0.01	0.59 ± 0.01	0.58 ± 0.01	0.57 ± 0.01	0.57 ± 0.01	0.58 ± 0.01	0.56 ± 0.01
Decay tau, ms	4.4 ± 0.2	3.7 ± 0.1	3.8 ± 0.2	3.8 ± 0.1	3.8 ± 0.1	3.7 ± 0.1	4.0 ± 0.1	3.5 ± 0.1
Frequency, Hz	1.8 ± 0.2	2.3 ± 0.1	2.3 ± 0.2	2.0 ± 0.2	1.5 ± 0.2	1.8 ± 0.2	2.0 ± 0.2	2.3 ± 0.3
N	31	39	36	46	31	31	24	24

All data are represented as mean ± SEM. Control for *hp255, †hp1168, and ‡hp1897. Rm, input resistance; Vm, resting potential; repla., replacement.